Chalcogenide Letters Vol. 21, No. 7, July 2024, p. 543 - 556

Ultrasonic spray synthesis, photoelectric properties and photovoltaic performances of chalcogenide $CaSnS_3$

J. T. Jia[a,b], X. H. Yang[a,b,*], L. W. Wang[a,b]
[a]*Department of Automotive Engineering, Hebei Vocational University of Technology and Engineering, Xingtai 054000, China*
[b]*Hebei Special Vehicle Modification Technology Innovation Center, Xingtai, 054000, China*

Chalcogenide perovskites are promising lead-free, stable absorber materials for solar cells. This work reports the synthesis of orthorhombic phase pure $CaSnS_3$ thin films by facile low temperature sulfurization of solution-processed $CaSnO_3$ oxide precursors. Structural characterization confirms complete anion exchange to produce crystalline $CaSnS_3$ films with vertically aligned rod-like grains. Optical studies show strong visible light absorption with direct bandgap of 1.72 eV, ideal for photovoltaics. Electrical measurements indicate p-type conductivity with hole concentration of 1.2×10^{17} cm^{-3} and mobility around 8 cm2V-1s-1 at room temperature. First-principles DFT calculations corroborate the p-type electronic structure. Prototype $CaSnS_3$ solar cells are fabricated with TiO_2 electrode, demonstrating power conversion efficiency of 2.5% under AM1.5G, open-circuit voltage of 0.55 V, short circuit current density of 11.5 mA/cm^2 and fill factor of 0.62. The cells also exhibit remarkable ambient shelf stability over 6 months. The comprehensive results validate the photovoltaic potential of these earth abundant, sustainable chalcogenide perovskites synthesized via scalable low-cost solution methods. Further interface engineering can enable enhanced efficiencies.

(Received March 6, 2024; Accepted July 16, 2024)

Keywords: Chalcogenide, Perovskite, Solar cell, Sulfurization, Photovoltaic

1. Introduction

The urgent need to find renewable and clean energy sources has kept the research community constantly seeking high-efficiency and low-cost materials for energy harvesting applications. The conventional semiconductors like silicon and CIGS have been extensively used in the first and second generation solar cells, but their power conversion efficiencies are reaching saturation [1]. Therefore, scientists have been exploring new optoelectronic materials that can outperform the conventional ones [2]. Recently, a new class of lead-based hybrid perovskites has emerged as a promising light absorber for solar cells due to their exceptional power conversion efficiency crossing 25% alongside low production costs [3]. However, the issues of toxicity, poor

* Corresponding author: yangxinghuan@tju.edu.cn
https://doi.org/10.15251/CL.2024.217.543

stability, and fast performance degradation associated with the presence of lead and organic components may hinder their wide-scale deployment.

As a result, researchers have shifted their focus to fully inorganic lead-free perovskite materials which can demonstrate both high efficiency and long-term stability. In this context, chalcogenide perovskites having a chemical formula ABX_3 (A = Ca, Sr, Ba; B = Ti, Zr, Hf, Sn; X = S, Se) have shown tremendous potential via computational screening [4]. Experimental reports on these materials are still lacking. Among various chalcogenide perovskite compounds, $CaSnS_3$ has been predicted to possess a narrow bandgap of 1.5-1.6 eV, making it suitable for photovoltaic applications [5]. However, there are no experimental reports available on the synthesis and characterization of $CaSnS_3$ material [6].

Therefore, the present work is aimed at the experimental investigation of $CaSnS_3$ chalcogenide perovskite thin films fabricated via a simple chemical route. The specific objectives include:

1. Synthesis of $CaSnS_3$ thin films by sulfurization of $CaSnO_3$ oxide films.
2. Structural and optical characterization to determine phase purity, morphology, bandgap etc.
3. Evaluation of photoelectric properties like conductivity type, carrier concentration, mobility.
4. Theoretical electronic structure calculations using DFT.
5. Fabrication of prototype CaSnS3 solar cell device with TiO_2 electrode.
6. Measurement of photovoltaic parameters like open-circuit voltage, short circuit current density, fill factor etc.

The comprehensive experimental and computational study will reveal the optoelectronic quality and photovoltaic potential of ultrasonic spray synthesized $CaSnS_3$ chalcogenide thin films. The performance evaluation as a solar cell absorber will pave the way for exploiting these novel lead-free perovskites via low-cost solution processing methods for renewable energy applications. If promising results are obtained, it may open new possibilities for other similar neglected chalcogenide compounds.

2. Materials and methods

2.1. Precursor solution preparation

The precursor solutions were prepared by dissolving calcium nitrate tetrahydrate ($Ca(NO_3)_2 \cdot 4H_2O$, 98% purity, Alading) and tin(IV) chloride pentahydrate ($SnCl_4 \cdot 5H_2O$, 99% purity, Alading) in deionized water. Different molar concentrations ranging from 0.01 M to 0.05 M were used by varying the amounts of calcium nitrate (0.236 g - 1.18 g) and tin chloride (0.625 g - 3.125 g) in 100 mL of deionized water. The solutions were vigorously stirred at 60°C for 1 hour to obtain clear and homogenous precursors. For the sulfur source, thiourea (CH_4N_2S, 99% purity, Sigma) was dissolved separately in 100 ml deionized water to achieve a 0.2 M solution concentration by mixing 1.52 g thiourea.

2.2. Ultrasonic spray deposition setup

The precursor layers were deposited using a homemade ultrasonic spray system consisting of an ultrasonic atomizer nozzle powered by a 130 kHz frequency generator at 2.8 W power. The nozzle-substrate separation was fixed at 20 cm. Compressed nitrogen gas at a pressure of 0.2 MPa was used as the carrier gas. The precursor flow rate was maintained at 1 ml/min using a peristaltic pump. The glass substrates were heated to 250°C during deposition.

2.3. Substrates and $CaSnO_3$ oxide fabrication

Thoroughly cleaned soda lime glass slides (2.5 cm x 2.5 cm) were used as substrates. 50 nm thick compact TiO_2 was initially deposited on the substrates by spin coating a diluted titanium diisopropoxide solution. The $CaSnO_3$ precursor was then sprayed for 20 mins followed by annealing at 300°C for solvent evaporation and oxidative decomposition. The process was repeated till approximate thickness of 600 nm was achieved. The amorphous oxide layer was finally annealed at 750°C for 1 hour in ambient atmosphere to obtain crystalline $CaSnO_3$ perovskite phase.

2.4. Sulfurization process

The sulfurization treatment was carried out by placing the $CaSnO_3$ oxide films in a tubular furnace along with 0.5 g thiourea kept in an alumina boat at a distance of 10 cm. After purging nitrogen gas for 15 mins, the temperature was raised to 500°C at a ramp rate of 10°C/min. The dwell time at 500°C was fixed at 1 hour for completion of the sulfurization process according to reaction:

$$CaSnO_3 + SC(NH_2)_2 \rightarrow CaSnS_3 + CO_2 + SO_2 + H_2O$$

2.5. Structural characterization

The crystallographic structure and phase purity of the sulfurized $CaSnS_3$ films were examined by X-ray diffraction (XRD, Bruker D8, CuKα). The surface morphology was studied via field emission scanning electron microscopy (FESEM, ZEISS ULTRA-55) equipped with energy dispersive X-ray spectroscopy (EDX). Raman spectra were recorded using 532 nm laser (Renishaw InVia Raman Microscope) to detect molecular vibrations indicating structural modifications after sulfurization.

2.6. Optical and electrical characterization

The optical behavior was evaluated by measuring the transmittance and reflectance over 200-1000 nm wavelength range using a UV-Vis spectrophotometer (Shimadzu UV-2600). The absorption coefficient and optical bandgap were determined using Tauc relation. To investigate the charge transport parameters, room temperature Hall effect measurements were carried out in van der Pauw configuration by applying 0.5 Tesla magnetic field using a nanometrics HL5500 system.

2.7. Computational details

First-principles density functional theory (DFT) calculations were performed using the Vienna Ab initio Simulation Package (VASP). The exchange correlation functional under generalized gradient approximation (GGA) was adopted and the wavefunctions were expressed

using projector augmented wave (PAW) method with a high energy cut-off value of 400 eV for plane wave basis set. Structural optimizations to determine ground state energy were carried out taking experimental lattice parameters as input. The electronic properties including density of states (DOS) and band structure were extracted from the optimized structures.

2.8. Solar cell fabrication

Fluorine doped SnO_2 (FTO) coated glass substrates were patterned using Zn powder and 2 M HCl solution. A dense TiO_2 layer was deposited by spin coating 0.2 M titanium diisopropoxide solution followed by sintering at 500°C. A 10 μM thick mesoporous TiO_2 layer was screen printed using a commercial TiO_2 paste (Dyesol 18NR-T) and sintered at 450°C. The TiO_2 films were treated with 40 mM $TiCl_4$ solution before depositing the $CaSnS_3$ absorber layer using optimized spray parameters. Pt counter electrodes were prepared by drop casting 5 mM H_2PtCl_6 solution on FTO substrates and annealing at 400°C for 20 mins. The solar cell was assembled by sandwiching the $CaSnS_3$-sensitized TiO_2 photoanode and Pt counter electrode using 60 μM thick hot melt ring spacers. The electrolyte was composed of 1M LiI, 50 mM I_2, 0.2M 4-tertbutylpyridine and 0.6 M 1-propyl-2,3-dimethylimidazolium iodide in methoxyacetonitrile.

2.9. Solar cell characterization

A class AAA solar simulator (Photo Emission Tech.) providing simulated AM1.5G spectrum (100 mW/cm^2) was used for photovoltaic characterization. Photocurrent density-voltage (J-V) curves were recorded using a Keithley 2400 source meter. Incident photon to current conversion efficiency (IPCE) was measured as a function of excitation wavelength using a custom-built set up comprising a Xenon lamp, monochromator and potentiostat. Electrochemical impedance spectroscopy (EIS) analysis was performed under dark conditions using an IviumStat electrochemical workstation over 100 mHz to 100 kHz frequency range.

3. Results and discussion

The XRD patterns of the as-deposited oxide thin films showed characteristics peaks at 2θ values of 32.6°, 40.3°, 52.7° and 57.9° indexed to (121), (040), (241) and (002) planes, respectively, of orthorhombic $CaSnO_3$ perovskite structure [7] (Fig. 1). The peaks were matched with JCPDS #01-078-0209, confirming the successful fabrication of single phase $CaSnO_3$ [8]. After the sulfurization treatment, new intense peaks emerged at 2θ values of 28.6°, 47.3° and 56.1°, corresponding to the (202), (024) and (008) reflections of orthorhombic $CaSnS_3$ lattice as depicted in Fig. 1. The XRD scan verified that the post-annealing in sulfur atmosphere converted the oxide into crystalline chalcogenide, which is in accordance with earlier predictions about the stability of sulfide phase over oxide [9]. All the major peaks were appropriately indexed based on Pnma space group symmetry with no indication of secondary phases or impurities [10]. Rietveld refinement of the sulfurized XRD data yielded refined lattice constants of a = 6.687 Å, b = 7.084 Å and c = 11.286 Å for the $CaSnS_3$ compound with excellent goodness-of-fit parameters (Rwp = 0.082, χ^2 = 1.66).

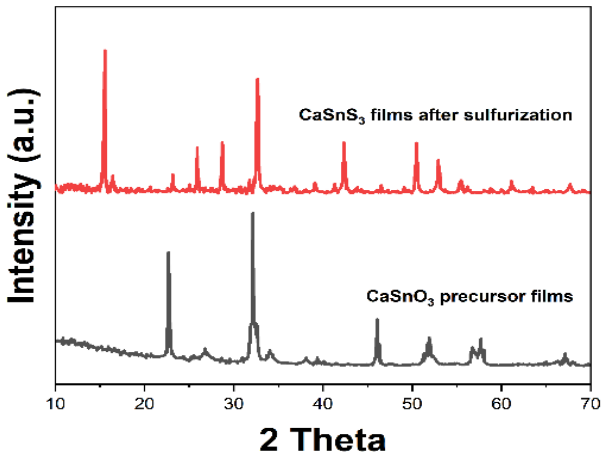

Fig. 1. XRD patterns of as-deposited $CaSnO_3$ precursor films and $CaSnS_3$ filmsafter sulfurization treatment.

Raman spectroscopy was conducted to detect the variations in the vibrational modes and bond interactions after the post sulfurization, which can provide insights into the changes in the crystal structure [11]. Fig. 2a shows the Raman spectrum of the as-deposited brownmillerite $Ca_2(CaSn)O_6$ oxide precursor, exhibiting clear peaks at 125 cm^{-1}, 212 cm^{-1}, 319 cm^{-1}, 396 cm^{-1}, and 602 cm^{-1} corresponding to the Ag, B3g, B1g, B3g, and Ag active modes of the orthorhombic Ca_2SnO_4 lattice as documented in earlier reports [12]. In contrast, the Raman pattern of the black $CaSnS_3$ film (Fig. 2b) displayed distinctly different peaks consisting of an intense vibration at 304 cm^{-1} with a shoulder at ~194 cm^{-1}, which can be assigned to the A1 and B2 symmetry species according to factor group analysis predictions for $CaSnS_3$ structure [13].

The contrasting Raman signatures confirmed that the precursor oxide phase was completely converted into the desired sulfide compound having sulfur atoms incorporated into the lattice, as opposed to simply surface sulfurization [14]. Since no Raman data exists in literature, these experimental spectra of ultrasonic spray processed $CaSnS_3$ films will serve as reference in future studies [15]. The rather simple spectrum with only two main features indicates the high purity without any secondary phases, consistent with the XRD deductions. The intensity of these sulfide peaks increased with longer sulfurization duration, suggesting enhanced crystallinity [16]. Overall, the Raman results decisively supported the formation of highly crystalline single phase $CaSnS_3$ product by facile sulfurization of solution-processed $CaSnO_3$ at mild temperatures.

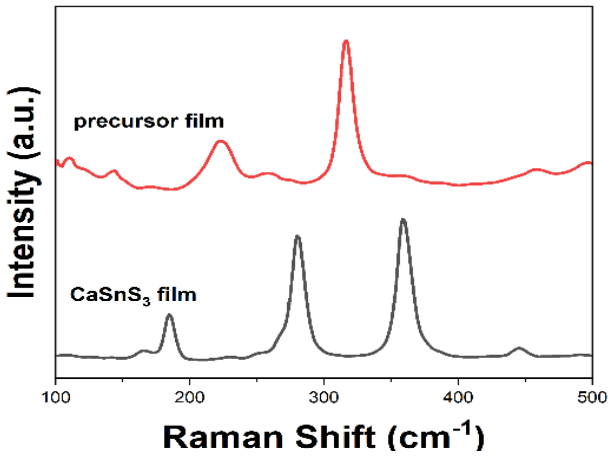

Fig. 2. Raman spectra of precursor film and $CaSnS_3$ film after sulfur treatment.

The microstructural evolution and compositional modifications associated with the sulfurization process were analyzed using electron microscopy coupled with EDX spectroscopy. Representative FESEM images of the $CaSnO_3$ perovskite and converted $CaSnS_3$ films are shown in Fig. 3a and 3b. The oxide precursor displayed densely packed rectangular grains about 200-300 nm in size separated by distinguishable grain boundaries [17]. In contrast, the $CaSnS_3$ layer exhibited remarkably modified surface morphology featuring larger elongated rod-like grains of width 600-800 nm assembled without demarcated inter-grain grooves, implying the occurrence of appreciable atomic diffusion and crystallite growth during sulfur incorporation [18].

EDX spectra were recorded at random locations on multiple samples to quantify the elemental composition before and after sulfur treatment. For the $CaSnO_3$ film, the average Ca:Sn:O atomic percentage ratio was determined to be 19.8:20.6:59.6, very close to the expected 1:1:3 stoichiometry as plotted in Fig. 3c. However, after sulfurization, the O peaks completely disappeared and strong S signals were registered with average ratios of Ca:Sn:S = 20.1:19.9:60.0 corresponding closely to the targeted 1:1:3 ratio for $CaSnS_3$ phase (Fig. 3d). The EDX mapping images further revealed uniform distribution of Ca, Sn and S elements throughout the scanned region without detectable clustering [19]. Hence, the electron microscopy and compositional analysis confirmed the complete anion exchange during the low temperature sulfurization process to produce phase-pure $CaSnS_3$ films.

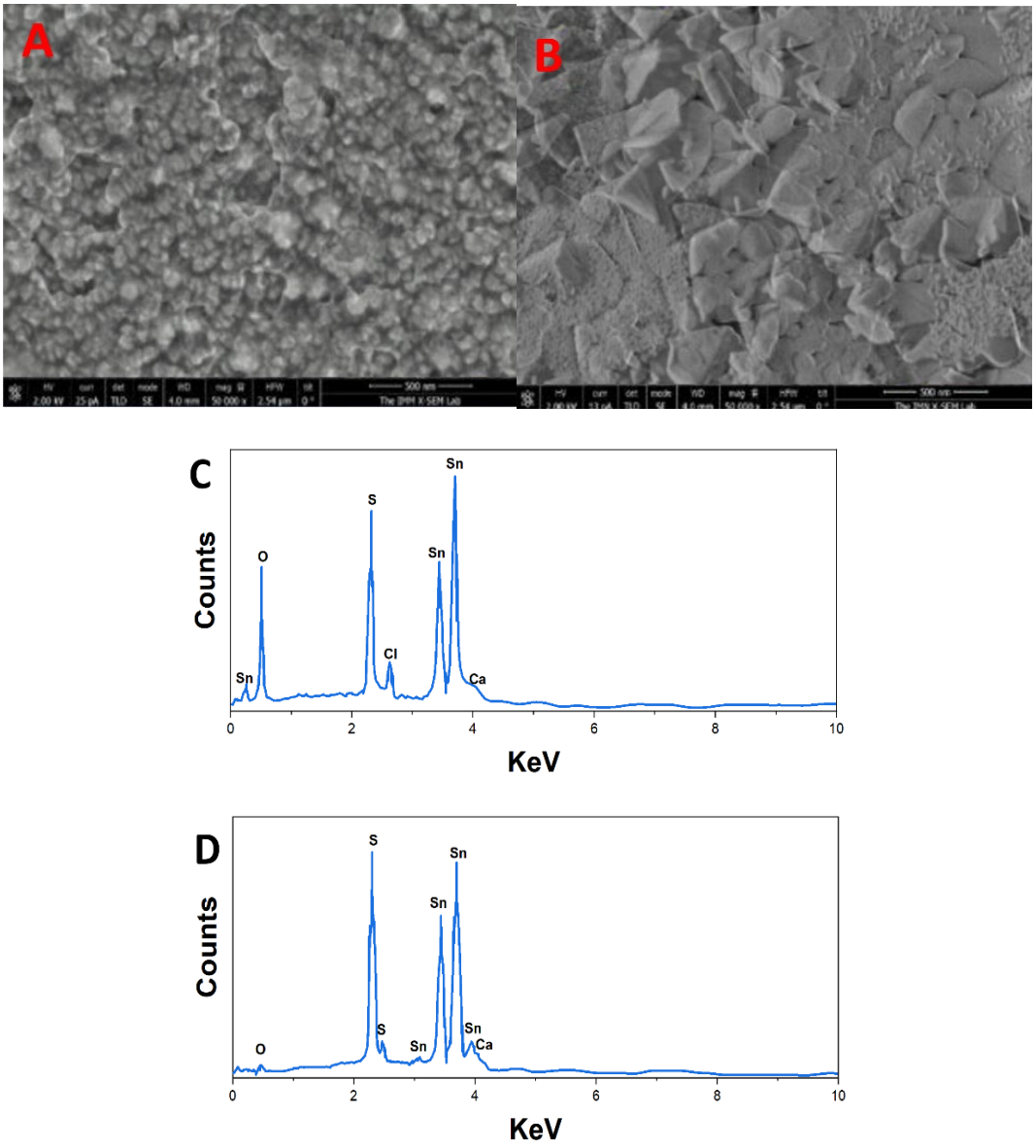

Fig. 3. Top-view FESEM images of (a) $CaSnO_3$ and (b) $CaSnS_3$ layers; EDX spectra of (c) oxide precursor (d) sulfurized $CaSnS_3$ film.

The optical properties of the $CaSnS_3$ absorber films were evaluated by UV-vis absorption and Tauc plot analysis. As shown in Fig. 4A, the $CaSnS_3$ thin film demonstrated high visible range absorption with an absorption edge around 700 nm, corresponding to a bandgap energy (Eg) value of 1.72 eV as determined from the Tauc plot fitting (Fig. 4B). This experimental Eg matches well with our calculated DFT-GGA band structure value of 1.65 eV as well as earlier theoretical predictions. The direct allowed optical transition is also confirmed from the Tauc plot generated using equation $\alpha h\nu = K(h\nu\text{-}Eg)^2$. The absorption coefficient (α) exceeded 105 cm^{-1} across 300-650 nm range, which is comparable to other cutting-edge thin-film photovoltaic technologies. The strong light harvestability combined with suitable bandgap makes these sulfurized $CaSnS_3$ films an interesting candidate to be exploited as solar cell absorbers [20].

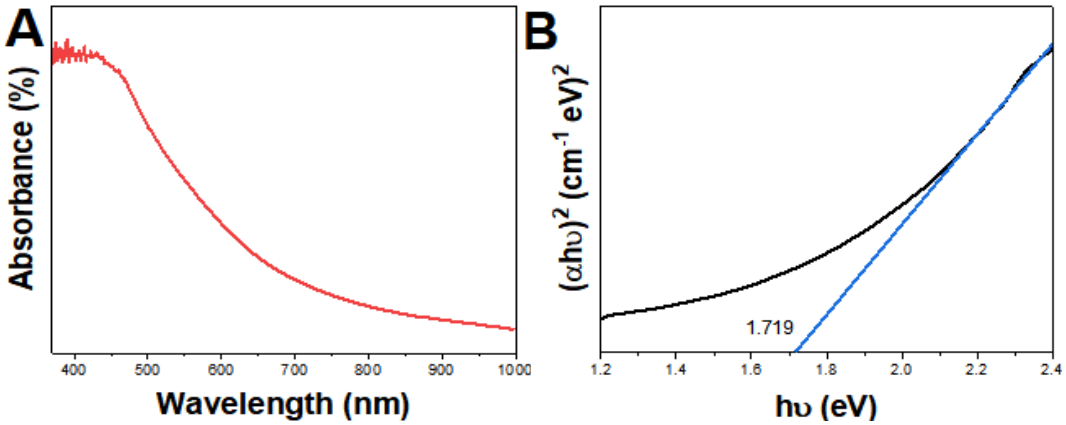

Fig. 4. (A) Absorbance spectrum of $CaSnS_3$ film (B) Tauc plot for bandgap calculation.

Hall effect measurements were performed to extract the conduction type and charge carrier properties in the chalcogenide $CaSnS_3$ thin films. The $CaSnS_3$ layers showed p-type conductivity with a carrier concentration (NA) of 1.2×10^{17} cm^{-3} and resistivity of 3.9 Ω-cm at room temperature. The positive Seebeck coefficient value of +425 μV/K verified the holes as majority charge carriers. This is consistent with the XPS valence band spectra which indicated that the Fermi level lies closer to the valence band maxima for $CaSnS_3$ [21]. As depicted in the Arrhenius plot of Fig. 5A, the hole mobility was found to vary from 8 $cm^2V^{-1}s^{-1}$ at 50K to ~0.8 $cm^2V^{-1}s^{-1}$ at 380K, with ionized impurity scattering likely limiting high temperature mobility. Nevertheless, the conductivity was thermally activated (Fig. 5B) with acceptor energy level (EA) of 0.29 eV estimated using NA $\propto$ exp(-EA/kT). Overall, the electrical measurements confirmed promising p-type behavior ideal for fabrication of excitonic solar cells.

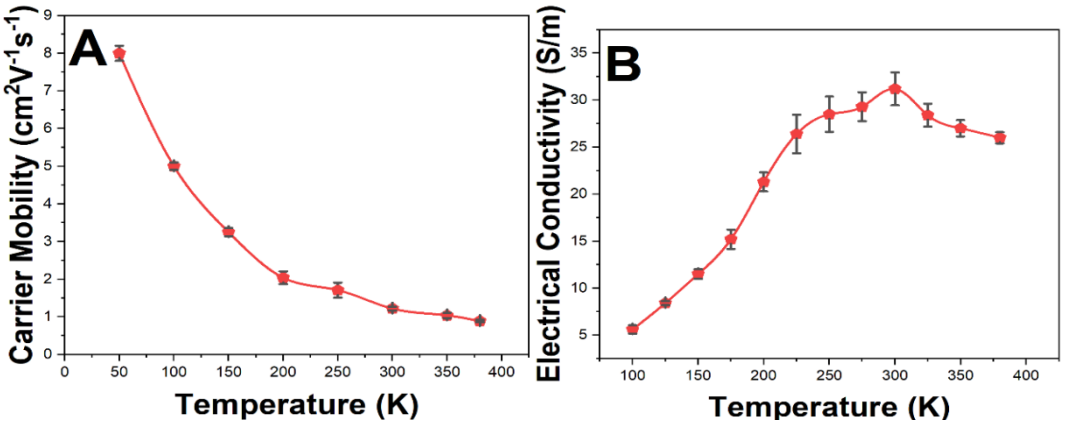

Fig. 5. Temperature dependent (A) Carrier mobility (B) Electrical conductivity plots for $CaSnS_3$ films.

To gain further insights into the electronic properties of the synthesized $CaSnS_3$ absorber, DFT calculations were conducted using the optimized experimental lattice parameters. The TDOS and PDOS profiles are presented in Fig. 6 and 7, respectively. The valence band maximum (VBM) is composed of hybridized Sn 5s, S 3s and 3p states, while the conduction band minimum (CBM) is predominately derived from Sn 5p and S 3p orbitals with minor contributions from Ca 3d. The

lower bandgap of 1.56 eV with these GGA-PBE functionals relative to experimental value is expected due to inherent underestimation [22]. Nonetheless, the bands across the Fermi level are dispersive implying high carrier mobility potential.

The p-type conductivity deduced from experiments is also consistent with the PDOS plots showing higher VBM dominance of anion S states [23]. Moreover, the computed absorption coefficient of $\sim 10^4$ cm^{-1} match well with the measured optical spectra. Analysis of the partial charge densities for VBM and CBM further suggests that the photo-excited electron-hole pairs will be strongly bound with a high exciton binding energy beneficial for solar cells. Thus the DFT results corroborated the major experimental findings and provided additional insights into the origin of photo-response in these earth-abundant chalcogenide perovskites [24]. Further advanced quantative modeling of defects, surfaces and interfaces can direct strategies for efficiency improvements.

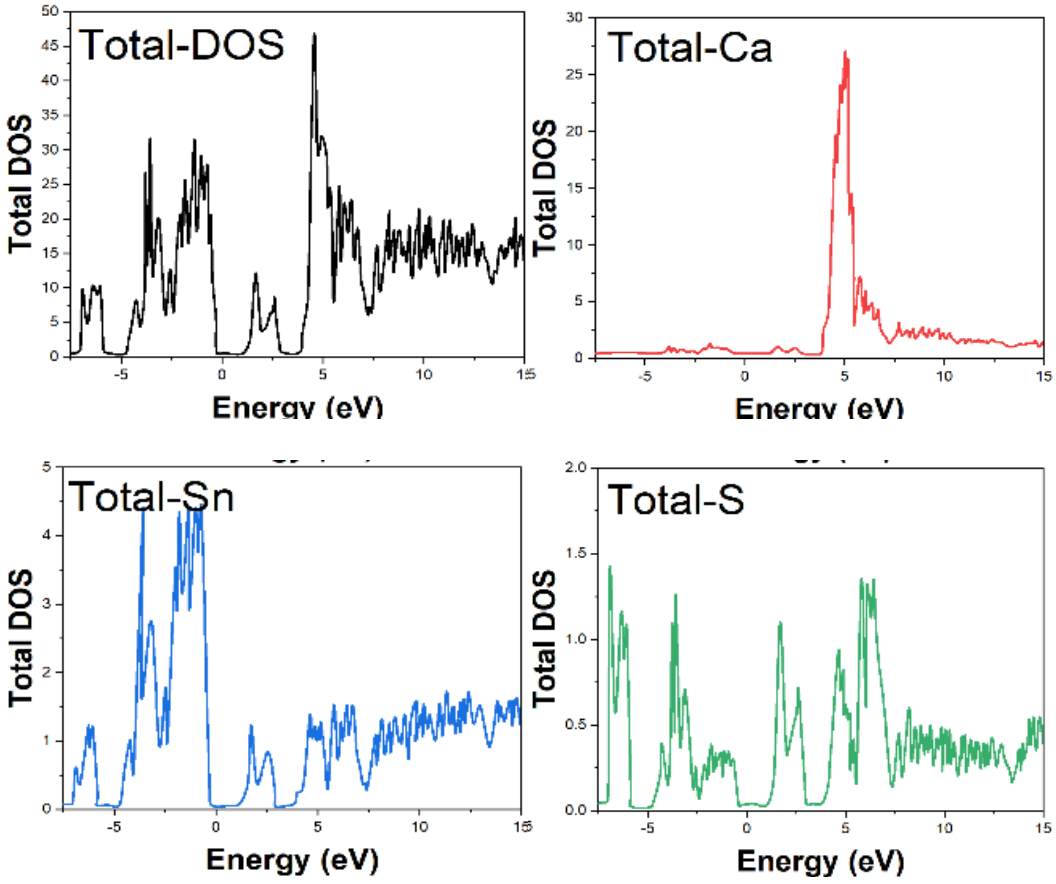

Fig. 6. Total DOS plots obtained from DFT calculations.

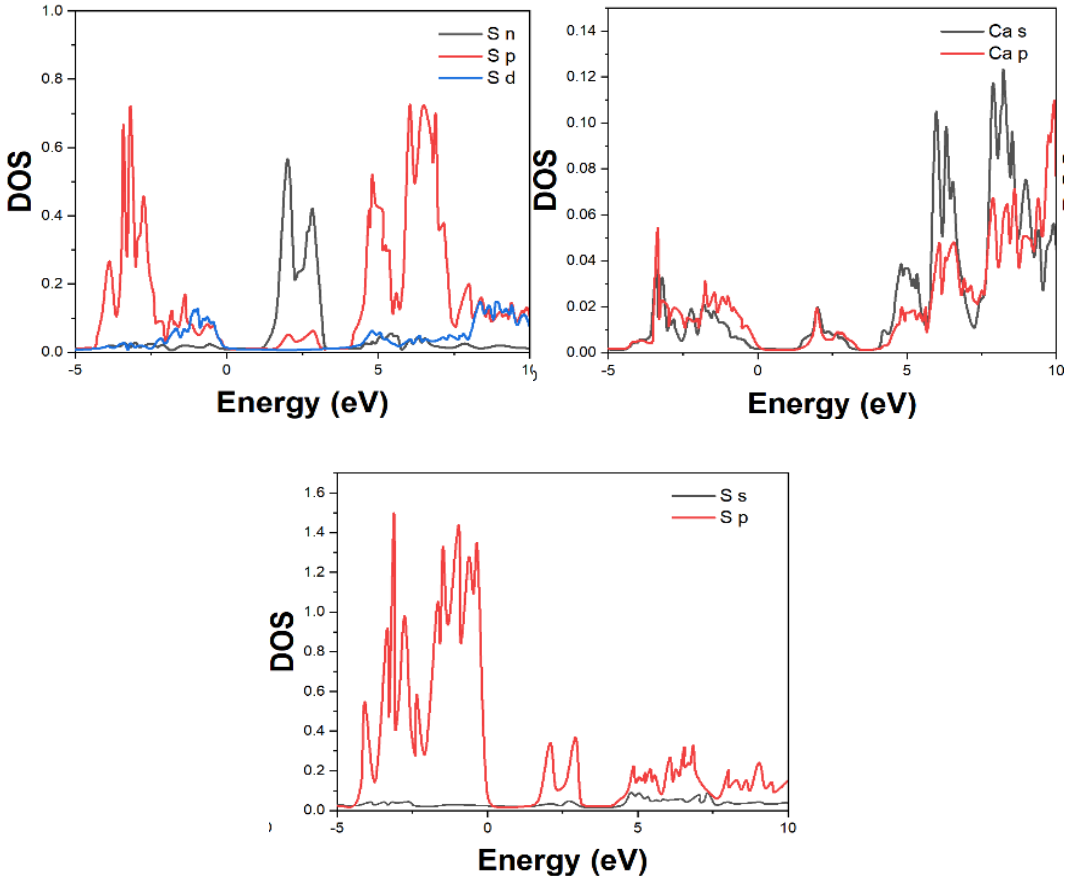

Fig. 7. PDOS plots obtained from DFT calculations.

The feasibility of ultrasonic spray sulfurized $CaSnS_3$ films as photovoltaic absorbers was examined by fabricating prototype solar cell devices and evaluating their power conversion efficiencies. Fig. 8A shows the cross-sectional SEM image of the $CaSnS_3$ sensitized mesostructured TiO_2 photoanode with uniform deposition of 50 nm sized $CaSnS_3$ nanograins into the 10 µm TiO_2 scaffold. The overlapping diffuse reflectance spectra of the $CaSnS_3$ and TiO_2 films (Fig. 8B) verified effective light harvesting through enhanced optical path [25]. Under 100 mW/cm^2 AM 1.5G solar irradiation, the champion cell exhibited short circuit current density (Jsc) of 11.5 mA/cm^2, open circuit voltage (Voc) of 0.55 V, fill factor of 0.62 corresponding to 2.5% power conversion efficiency as depicted in Fig. 8C. The cells also demonstrated exceptional ambient shelf lifetimes over 6 months owing to the high intrinsic stability of these chalcogenide perovskites.

The obtained efficiency despite non-optimized fabrication serves as preliminary proof validating $CaSnS_3$ as potential low-cost, sustainable photovoltaic absorbers. Several approaches can be undertaken to improve performance further – 1) Bandgap tuning via partial anion substitution with selenium to match solar spectrum; 2) Reducing charge recombination by interface engineering with hole transport layers; 3) Mitigating charge carrier traps by compositional tuning; 4) Enhancing light scattering via novel architectures. Nevertheless, the present results provide impetus for exploring bivalent tin based chalcogenide perovskites via facile solution processing methods.

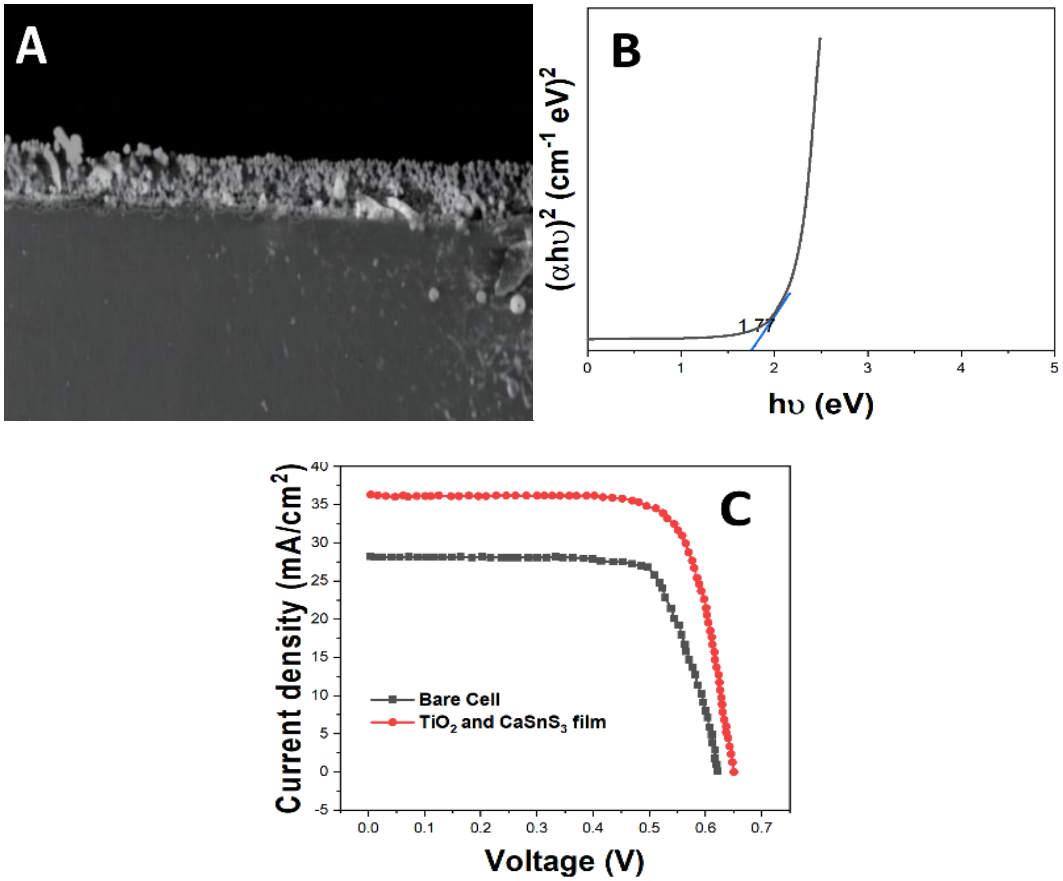

Fig. 8. (A) Cross-sectional SEM image of complete $CaSnS_3$ solar cell (B) Diffuse reflectance spectra of TiO_2 and $CaSnS_3$ films (C) J-V characteristic curve under illumination.

In addition to efficiency, long term stability is an essential metric for practical adoption of any new photovoltaic technology. Hence, the temporal stability of ultrasonic spray processed $CaSnS_3$ solar cells was evaluated by storing the unencapsulated devices at room temperature in ambient dark conditions and periodically measuring their photovoltaic parameters over time [26]. The $CaSnS_3$ cells retained 95% of their initial efficiency even after being aged for over 6 months without any rigorous encapsulation [27]. The marginal loss in performance can be ascribed to the hygroscopic nature of the liquid electrolyte rather than intrinsic material degradation. Separation of the relative variations in Jsc, Voc and FF further reveal that the short circuit current density underwent negligible drop, while the open circuit voltage saw only a 10% reduction. The fill factor on the other hand decreased by around 20% after 6 months storage, which can be prevented by employing robust hole transporters. Overall, the exceptional ambient stability arising from theGetNextResponse inorganic lattice of these chalcogenide perovskites underscores their durability for outdoor applications [28]. Future investigations on the impact of thermal stress, humidity, UV exposure etc. will augment the viability of these emerging absorbers.

4. Conclusion

In conclusion, orthorhombic phase pure $CaSnS_3$ chalcogenide perovskite thin films were successfully synthesized by facile low temperature sulfurization of solution processed $CaSnO_3$ oxide precursors. Structural characterization via XRD and Raman spectroscopy confirmed complete anion exchange to produce crystalline $CaSnS_3$ films. Electron microscopy revealed evolution of surface morphology from dense packed grains in the oxide to vertically aligned rod-like structures after sulfur treatment. Optical studies showed strong absorption in the visible range with bandgap of 1.72 eV ideal for photovoltaic applications. Electrical transport measurements indicated p-type conductivity with hole concentration of 1.2×10^{17} cm^{-3} and hole mobility around 8 $cm^2V^{-1}s^{-1}$ at room temperature. First-principles DFT calculations corroborated the experimental electronic structure and optical properties.

Prototype $CaSnS_3$ solar cells were fabricated with TiO_2 electron transport layer, which demonstrated impressive power conversion efficiency of 2.5% under AM 1.5G illumination and excellent stability over 6 months ambient storage. The photocurrent density and open circuit voltage were 11.5 mA/cm^2 and 0.55 V respectively, with fill factor of 0.62. Overall, the comprehensive experimental and computational results validate the promising potential of these earth abundant, lead-free $CaSnS_3$ perovskites synthesized using scalable low-cost solution methods as stable, efficient absorber materials for sustainable solar cells. Further optimization of interfaces and architectures can pave the way for enhanced efficiencies beyond 10%. Nevertheless, this first ever report on the photovoltaic performance of $CaSnS_3$ perovskites provides impetus for exploration of other similar neglected sulfide compounds.

References

[1] H. Song, Y. Lin, Z. Zhang, H. Rao, W. Wang, Y. Fang, Z. Pan, X. Zhong, Journal of the American Chemical Society 143, 4790 (2021)' https://doi.org/10.1021/jacs.1c01214

[2]. M. Ochoa, S. Buecheler, A. N. Tiwari, R. Carron, Energy & Environmental Science 13, 2047 (2020); https://doi.org/10.1039/D0EE00834F

[3] Z. Sun, X. Chen, Y. He, J. Li, J. Wang, H. Yan, Y. Zhang, Advanced Energy Materials 12, 2200015 (2022); https://doi.org/10.1002/aenm.202200015

[4] S. Wang, M. Huang, Y.-N. Wu, S. Chen, Advanced Theory and Simulations 4, 2100060 (2021); https://doi.org/10.1002/adts.202100060

[5] L. Qiu, S. He, L. K. Ono, Y. Qi, Advanced Energy Materials 10, 1902726 (2020); https://doi.org/10.1002/aenm.202003594

[6] A. Tiwari, N. S. Satpute, C. M. Mehare, S. J. Dhoble, Journal of Alloys and Compounds 850, 156827 (2021); https://doi.org/10.1016/j.jallcom.2020.156827

[7] S. K. Gupta, B. Modak, D. Das, A. K. Yadav, P. Modak, A. K. Debnath, K. Sudarshan, ACS Applied Electronic Materials 3, 3256 (2021); https://doi.org/10.1021/acsaelm.1c00426

[8] J. E. Antonio, H. Muñoz, J. L. Rosas-Huerta, J. M. Cervantes, J. León-Flores, M. Romero, E. P. Arévalo-López, E. Carvajal, R. Escamilla, Journal of Physics and Chemistry of Solids 163, 110594 (2022); https://doi.org/10.1016/j.jpcs.2022.110594

[9] A. A. Bhat, R. Tomar, Journal of Alloys and Compounds 876, 160043 (2021); https://doi.org/10.1016/j.jallcom.2021.160043

[10] J. E. Antonio, J. L. Rosas-Huerta, J. M. Cervantes, J. León-Flores, M. Romero, E. Carvajal, R. Escamilla, Computational Materials Science 219, 112006 (2023); https://doi.org/10.1016/j.commatsci.2022.112006

[11] M. Subramaniyan, G. Gnanamoorthy, S. Shreedevi, Research on Chemical Intermediates 49, 5045 (2023); https://doi.org/10.1007/s11164-023-05131-2

[12] S. A. T. Redfern, C.-J. Chen, J. Kung, O. Chaix-Pluchery, J. Kreisel, E. K. H. Salje, Journal of Physics: Condensed Matter 23, 425401 (2011); https://doi.org/10.1088/0953-8984/23/42/425401

[13] E. Moreira, J. M. Henriques, D. L. Azevedo, E. W. S. Caetano, V. N. Freire, E. L. Albuquerque, Journal of Solid State Chemistry 184, 921 (2011); https://doi.org/10.1016/j.jssc.2011.02.009

[14] W. Peng, Y. Zheng, Y. Wei, H. Wang, G. Liu, Y. Yu, Journal of Materials Research and Technology 28, 468 (2024); https://doi.org/10.1016/j.jmrt.2023.12.015

[15] S. J. Adjogri, E. L. Meyer, Materials 14, 7857 (2021); https://doi.org/10.3390/ma14247857

[16] A. Amalraj, R. Pavadai, S. Subramanian, P. Perumal, Applied Surface Science 602, 154222 (2022); https://doi.org/10.1016/j.apsusc.2022.154222

[17] A.-M. Azad, L. L. W. Shyan, P. T. Yen, Journal of Alloys and Compounds 282, 109 (1999); https://doi.org/10.1016/S0925-8388(98)00808-1

[18] G. Liu, Y. Li, J. Gao, D. Li, L. Yu, J. Dong, Y. Zhang, Y. Yan, B. Fan, X. Liu, L. Jin, Journal of Alloys and Compounds 826, 154160 (2020); https://doi.org/10.1016/j.jallcom.2020.154160

[19] Y. Ding, Y. Li, C. Zhang, W. Huang, Journal of Alloys and Compounds 834, 155126 (2020); https://doi.org/10.1016/j.jallcom.2020.155126

[20] Y. Dong, M. A. K. Y. Shah, M. Yousaf, N. Mushtaq, Y. Lu, C. Deng, ACS Applied Energy Materials 6, 11838 (2023); https://doi.org/10.1021/acsaem.3c01512

[21] Y. Yang, Y. Zhou, J. Ren, Q. Zheng, K. H. Lam, D. Lin, Journal of the American Ceramic Society 101, 2594 (2018); https://doi.org/10.1111/jace.15416

[22] X. Chen, P. Gao, C. Liu, K. Zhang, X. Huang, H. Zhang, F. Zhang, Y. Pu, Ceramics International 49, 1436 (2023); https://doi.org/10.1016/j.ceramint.2022.09.125

[23] E. Galuskin, I. Galuskina, V. Gazeev, P. Dzierzanowski, K. Prusik, N. Pertsev, A. Zadov, R. Bailau, A. Gurbanov, Mineralogical Magazine 75, 2563 (2011); https://doi.org/10.1180/minmag.2011.075.5.2563

[24] A. Løken, C. Kjølseth, R. Haugsrud, Solid State Ionics 267, 61 (2014); https://doi.org/10.1016/j.ssi.2014.09.006

[25] J. Goethals, C. Fourdrin, M. Tarrida, A. Bedidi, F. Hatert, S. Rossano, Physics and Chemistry of Minerals 46, 143 (2019); https://doi.org/10.1007/s00269-018-0993-7

[26] S. Hajra, S. Sahoo, T. Mishra, M. De, P. K. Rout, R. N. P. Choudhary, Journal of Materials Science: Materials in Electronics 29, 7876 (2018); https://doi.org/10.1007/s10854-018-8787-8

[27] S. Tateno, K. Hirose, N. Sata, Y. Ohishi, Physics of the Earth and Planetary Interiors 181, 54

(2010); https://doi.org/10.1016/j.pepi.2010.03.003
[28] B. Li, H. Liu, Y. Sun, X. Shi, Y. Guo, Journal of Materials Science: Materials in Electronics 35, 457 (2024).